222
8-11-81

JULY 1981

PPPL-1817
UC-20A,D,G

DL-2933
B6359

MASTER

IDEAL AND RESISTIVE MHD STABILITY OF ONE-DIMENSIONAL TOKAMAK EQUILIBRIA

BY

M.S. CHANCE, H.P. FURTH,
A.H. GLASSER, AND H. SELBERG

PLASMA PHYSICS LABORATORY

PRINCETON UNIVERSITY
PRINCETON, NEW JERSEY

This work was supported by the U.S. Department of Energy Contract No. DE-AC02-76-CHO 3073. Reproduction, translation, publication, use and disposal, in whole or in part, by or for the United States government is permitted.

Ideal and Resistive MHD Stability of One-Dimensional Tokamak Equilibria

M. S. Chance, H. P. Furth, A. H. Glasser,*
and H. Selberg

Princeton Plasma Physics Laboratory
Princeton University
Princeton, NJ 08544

Abstract

The MHD equilibrium and stability of a vertically elongated tokamak configuration are analyzed in the one-dimensional limit corresponding to infinite elongation. Stability against all ideal MHD modes can be obtained for beta-values arbitrarily close to unity. In the finite-resistivity stability analysis, axisymmetric ($m = 0$) tearing modes, centered on the null trace of the poloidal field, can be stabilized by a loosely fitting conducting shell. The presence of the toroidal field component, however, introduces the possibility of nonsymmetric tearing modes ($m \neq 0$), centered away from the null trace. These modes can be stabilized only by a more tightly-fitting shell, plus reliance on finite-pressure effects on the small-major-radius side of the plasma profile. Under these conditions, stable configurations with peak beta values approaching unity are readily found.

*Present Address: Physics Department, Auburn University, Auburn, Alabama 36830

I.

Axially elongated two-dimensional tokamak configurations have been studied exhaustively, with a view to maximizing the plasma beta value [1-7]. In this process, ideal-MHD-stable configurations with appreciable beta-values have been demonstrated, but the sharply peaked plasma-current distributions that emerge in this type of optimization process are conducive to finite-resistivity tearing modes. A systematic finite-resistivity, finite-beta analysis has not as yet been carried out for two-dimensional tokamaks [8], but the range of stable beta values attainable with "realistic" current profiles seems unlikely to exceed 0.1. The most promising results are obtained with finite but moderate vertical elongations.

The stability properties of an infinitely elongated one-dimensional tokamak might be expected to differ considerably from those of a two-dimensional tokamak with a large but finite degree of vertical elongation. The present paper shows that the high-beta stability properties may in fact be much more favorable. The results are directly applicable to some tokamak-like fast-pulsed configurations that have approximately one-dimensional central regions, such as a highly elongated belt pinch or a reversed-field theta pinch with added toroidal field.

In view of the strong attraction of the stable high-beta solutions of the one-dimensional tokamak, one is also led to envisage the possibility of an experimental tokamak embodiment where a highly extended mid-section is held in equilibrium (i.e., under tension) by two appropriately shaped two-dimensional *end sections*. The equilibrium and stability conditions of these end sections would be expected to call for non-Maxwellian features -- a kind of "tandem tokamak." The present paper addresses only the long central region, where the profiles depend on r and not on z.

In Sec. II we describe how the equilibrium is calculated and discuss some of its properties. Section III contains the stability analysis in which the significant parameters of the equilibrium are optimized for stability against both ideal MHD and resistive tearing modes. Section IV contains the conclusion and we include a brief qualitative discussion of the consequences of taking the required two-dimensional end sections into account.

II. Equilibrium

The model is depicted in Fig. 1. In the cylindrical polar coordinate system (r, ϕ, z) the central plasma region is contained within an annulus defined by $r_1 < r < r_2$ and is separated by a vacuum region from conducting shells situated at $r = a, b$. Note that in our model the magnetic axis now becomes a null trace at $r = r_0$, across which the poloidal field, B_p, changes direction. This configuration would be essentially that of a belt pinch, or a hard core reversed field pinch if the roles of the poloidal and toroidal field were interchanged. The results of this paper can thus be of some significance to these devices.

Although the equilibrium equations for the one-dimensional case can be reduced to quadratures, we instead solve the usual Grad-Shafranov equation for the poloidal flux, $\Psi = 2\pi\psi(r)$, with the pressure, p, and the toroidal field function, g, specified to be functions of ψ only as is generally done for tokamak equilibria. If

$$\underline{B} = \nabla\phi \times \nabla\psi + g(\psi)\nabla\phi \quad , \tag{1}$$

then we have

$$r \frac{d}{dr} \frac{1}{r} \frac{d}{dr} y = - \frac{1}{\psi_b^2} \left(g \frac{dg}{dy} + r^2 \frac{dp}{dy} \right) = \frac{r j_\phi}{\psi_b} \quad , \tag{2}$$

where $\psi_b = \psi(r_1) = \psi(r_2)$ and $y \equiv \psi/\psi_b$.

For the plasma profiles we choose, for $0 \leq y \leq 1$,

$$p(y) = p_o \frac{e^{\lambda_p (1 - y)^2} - 1}{e^{\lambda_p} - 1} \quad , \tag{3}$$

and

$$g(y) = g_o - g_1 \frac{e^{\lambda_g (1 - y)^2} - 1}{e^{\lambda_g} - 1} \quad , \tag{4}$$

so that the peak pressure and the diamagnetic contribution of the toroidal field is specified by p_o and g_1. Note that we can prescribe peaked, rounded, or flattened profiles in the physical coordinate, r, by choosing respectively, $\lambda >> 0$, $\lambda = -0.5$, or $\lambda << 0$. Since the first three derivatives of dp/dy with respect to r vanishes at r_o for $\lambda_p = -\frac{1}{2}$ then, when $g_1 = 0$ we have $j_\phi/r \propto - dp/dy$, and the corresponding profiles for j_ϕ/r are respectively peaked (or rounded), flat, and hollow. This is illustrated in Fig. 2, where we plot the pressure and current profiles for $\lambda_p = 1.0, 0, -0.5$, and -1.0. The extreme case when $\lambda_p \to -\infty$ gives a square pressure profile with a corresponding skin current. In addition, we prescribe r_o, r_2, g_o, and $B_p(r_2)$ so that the aspect ratio, $R \equiv r_o/(r_2 - r_o) \equiv r_o/d$, axial toroidal beta, $\beta_v \equiv 2p_o r_o^2/g_o^2$ (based upon the vacuum toroidal field at r_o), and poloidal beta, $\beta_p \equiv 2p_o/B_p^2(r_2)$.

We solve Eq. (2) for $y(r)$ in the region ($r_o < r < r_2$) numerically by initializing with

$$y(r_o) = 0 \quad ,$$

$$\frac{dy(r_o)}{dr} = 0 \quad ,$$

and iterating on g_1 and ϕ_b so that

$$y(r_2) = 1 \quad ,$$

and

$$\frac{dy(r_2)}{dr} = \frac{-r_2 B_p(r_2)}{\phi_b} \quad . \tag{5}$$

Equation (2) is then integrated backward for $y(r)$ and r_1 in the region ($r < r_o$) until $y(r_1) = 1.0$. This specifies r_1, and the equilibrium quantities there are calculated from Eqs. (1)-(4). Thus, some toroidal features, such as the idea of flux surfaces, and toroidal shift, are preserved in our model.

The solution in the vacuum region is readily obtained, i.e.,

$$y(r) = -\frac{B_p(r_p)}{2}\left(r^2 - r_p^2\right) + y\left(r_p\right) \quad , \tag{6}$$

where r_p is the value of r at either plasma boundary. This equation shows the tendency for flux surfaces to be spaced farther apart on the inner side of the magnetic axis. The final magnetic field profiles are stored as cubic spline functions to allow for interpolation and differentiation.

Instead of parametrizing the plasma by the safety factor, we find it convenient to use the pitch of the magnetic field defined by

$$\mu(r) \equiv - \frac{rB_p}{B_\phi} \quad , \tag{7}$$

and a rational surface is present when $m = k\mu$, m and k being respectively the toroidal and poloidal wave numbers.

Since rB_ϕ and B_p are both constant in regions exterior to the plasma, but $B_p \sim r - r_o$ inside the plasma, μ has at least one relative minimum in the plasma on the inner side of the null trace. As shown in Fig. 2, this means that, in the region $[a, r_\mu]$ where r_μ is defined by $\mu(r_\mu) = \mu(a)$, rational surfaces exist in pairs for the same values of m and k. This is relevant to the stability analysis which is described in the next section.

III. Stability

The stability properties of our model are analyzed for both ideal and resistive MHD modes. The underlying assumptions which enable us to treat our system in one dimension permit us to apply the fundamental results previously obtained from studies of the simpler slab, or cylindrical, systems. Thus, for ideal MHD modes we apply the results of Newcomb [9], Suydam [10] etc.; analysis of the resistive MHD modes is based upon the ideas found in Furth et al., [11], and Glasser et al., [12]. Newcomb's equations are relevant to both types of modes since sufficient conditions for stability against resistive modes can be obtained from the behavior of the plasma in the ideal regions. The relevant equations are the energy integral and the associated Euler-

Lagrange equation [9]

$$W(\xi) = \frac{\pi}{2} \int_a^b r dr \left[F \left(\frac{d\xi}{dr}\right)^2 + G \xi^2 \right] \tag{8}$$

$$F\xi' - \zeta = 0$$

$$\zeta' - G\xi = 0 \tag{9}$$

where

$$F = \frac{r(krB_p - mB_\phi)^2}{k^2r^2 + m^2} , \tag{10}$$

$$G = \frac{2k^2r^2}{k^2r^2 + m^2} \frac{dp}{dr} + \frac{1}{r} (krB_p - mB_\phi)^2 \frac{k^2r^2 + m^2 - 1}{k^2r^2 + m^2}$$

$$+ \frac{2k^2r}{(k^2r^2 + m^2)^2} (k^2r^2B_p^2 - m^2 B_\phi^2) , \tag{11}$$

with

$$2 \frac{dp}{dr} = - \frac{1}{r^2} \frac{d}{dr} (r^2B_\phi^2) - \frac{d}{dr} B_p^2 . \tag{12}$$

Equation (8) is, of course, the marginal ($\omega^2 = 0$) one dimensional version of the more general energy integral of Bernstein et al., [13]. The ϕ and z components of the plasma displacement which is assumed to have the form $\underline{\xi}(r)e^{i(kz - m\phi)}$, have been eliminated algebraically in the minimization of $W(\xi)$, so that ξ here is the radial component of the Fourier coefficient of of the displacement.

As shown by Newcomb [9], we can also write the energy integral in the form

$$W(\xi) = \frac{\pi}{2} \int_a^b r dr \left\{ \frac{1}{k^2 r^2 + m^2} \left[(krB_p - mB_\phi) \frac{d\xi}{dr} + (krB_p + mB_\phi) \frac{\xi}{r} \right]^2 \right.$$

$$\left. + \left[(krB_p - mB_\phi)^2 - 2\, B_\phi \frac{d}{dr} (rB_\phi) \right] \frac{\xi^2}{r^2} \right\} \tag{13}$$

showing explicitly, Rosenbluth's sufficient condition for stability against all ideal MHD modes: $W(\xi) > 0$ if rB_ϕ is a decreasing function of r throughout the plasma. For the purposes of this paper we take rB_ϕ = constant, i.e., $q_1 = 0$, thereby rendering our model ideally stable irrespective of the values of the other equilibrium parameters such as aspect ratio, wall position, profile shapes, etc. Note, however, that our condition $B_\phi \sim 1/r$ implies that the toroidal field is the vacuum field throughout so the plasma is contained entirely by the poloidal field, i.e., the poloidal beta, $\beta_p \sim 1$, while the total plasma beta $\beta \sim \beta_p (1 + B_\phi^2/B_p^2)^{-1}$ can, in principle, be arbitrarily close to unity and still be stable against all ideal MHD modes.

We investigate the resistive MHD properties of our system in the usual way: resistive effects are important only in the region where Eq. (9) is singular, i.e., at the rational surfaces where $m = k\mu$, but a sufficient condition for stability can be obtained by examining the discontinuity in the Euler-Lagrange solution across the singularity. The solution of Eq. (9) in the ideal region on the right, left of a singularity at $r = r_s$, can be written,

$$\begin{pmatrix} \xi(r) \\ \zeta(r) \end{pmatrix}_{R,L} = \begin{pmatrix} \xi_\ell & \xi_s \\ \zeta_\ell & \zeta_s \end{pmatrix}_{R,L} \begin{pmatrix} A \\ B \end{pmatrix}_{R,L} \tag{14}$$

where $\xi_\ell(r)$, $\xi_s(r)$ are the solutions which, in Newcomb's definition, are large, small at $r = r_s$. Thus, A_R and B_R are the contributions from the solution at the right of the singularity. If A_L and B_L are similarly defined, a sufficient condition for stability against resistive modes is that [12]

$$\Delta' \equiv \frac{B_R}{A_R} + \frac{B_L}{A_L} < 0 \quad . \tag{15}$$

We note here that this condition encompasses the cases where $p'(r)$ can be either finite or zero, it being also a necessary condition for the latter. Inversion of the set of Eq. (14) gives

$$\begin{pmatrix} A \\ B \end{pmatrix}_{R,L} = \begin{pmatrix} \xi_\ell & \xi_s \\ \zeta_\ell & \zeta_s \end{pmatrix}^{-1}_{R,L} \begin{pmatrix} \xi(r) \\ \zeta(r) \end{pmatrix}_{R,L} \quad . \tag{16}$$

Here ξ_ℓ, ξ_s, ζ_ℓ, ζ_s are obtained analytically as a power series about the singular surface, r_s. The details of this expansion and an estimate of the accuracy of the method are shown in the Appendix. We use an accurate extrapolative differential equation solver [14] to integrate Eq. (9) towards r_s with the boundary conditions $\xi(a) = \xi(b) = 0$, $\zeta(a) = \zeta(b) = 1.0$. In the process, the A, B as calculated by Eq. (16) approach their constant values as $r \to r_s$. The point up to which we integrate is, of course, determined by the number of terms in the indicial expansion and the required accuracy for A, B. On the other hand, numerical considerations dictate that we keep a respectable distance away from the singularity.

For each set of equilibrium parameters we choose the toroidal mode number m and the rational surface r_s, determine the poloidal wave vector through

$$k = m/\mu(r_s) \quad , \tag{17}$$

and then compute Δ' as described above. For these modes, we present the results graphically by showing plots of $\Delta' d$, versus r_s for various values of wall position, profile shapes, plasma beta and aspect ratio. The quantity $\Delta' d$ is dimensionless when the pressure is zero. Because of the existence of the double tearing region as discussed in the last section, we do *not present results for $\Delta' d$ in $[a, r_\mu]$.* There, the solution of Eq. (9) must be properly matched across the bounding resistive layers. To realize this, we would require knowing the threshold value of $\Delta' d$ or details of the perturbation inside the layers.

The effect of a conducting wall on the m = 1 and 2 modes is shown in Fig. 3a for a flat current profile ($\lambda_p = -0.5$), aspect ratio R = 5, $r_0 = 10.0$, $r_2 = 12.0$, and $\beta_v = 16\%$ [$p_o = 0.08$, $B_r(r_2) = -0.4$, $g_o = 10.0$]. It is seen that Δ' can be made negative for all values of $r > r_o$, i.e., over the entire region of unfavorable curvature, if the wall is positioned within 0.2d of the plasma boundary. The value of $\Delta' d$ is positive and becomes large in the region where the pitch, μ, has a minimum. This may seem dangerous, but it should be noted that the curvature is favorable for stability in this region, and it is expected that the threshold Δ', i.e., Δ_c, will also be large and positive there. In Fig. 3b we plot similar curves for a larger value of β, i.e., p_o = 0.5, $B_p(r_2) = -1.0$ so that $\beta_v = 1.0$. In both figures, the m = 1 mode (solid line) is more unstable than the m = 2 mode (dashed line) [15]. Note that Δ' is fairly insensitive to the value of β_v.

The effect of the profile shape is shown in Fig. 4a for peaked (λ_p = 1.0), rounded ($\lambda_p = 0$), flat ($\lambda_p = -0.5$), and hollow ($\lambda_p = -1.0$) current profiles. The wall position is kept at 0.2d and β_v is 16% [p_o = 0.08, $B_p(r_2)$ = -0.4]; the other equilibrium parameters are the same as above. It is seen that the flat profile is the most stable; this current shape is characterized by having its gradient, the driving force of the resistive kink, near the plasma boundary and hence near to the strong stabilizing effect of the conducting shell. For the hollow profile case the current gradient becomes very steep and the wall must be brought in closer than that shown in order to provide the same degree of stabilization. Figure 4b shows the results for β_v = 1.0 as in Fig. 3, showing again the relative insensitivity of $\Delta'd$ to the plasma beta.

In Fig. 5 we show the effect of varying the plasma beta for the flat profile ($\lambda_p = -0.5$), the wall again at 0.2d and an aspect ratio of 5. Curves of $\Delta'd$ for β_v of 0.16, 1.0, and 100.0 [p_o = 50.0, $B_p(r_2)$ = -10.0] are shown. These correspond to β^* of 9.3%, 32.6%, and 64.5% respectively where

$$\beta^* = 2p^*/[B_\phi^2(r_o) + B_p^2(r_2)] \quad ,$$

$$p^* = \left[\int p^2 dv/\int dv\right]^{1/2} \quad . \tag{18}$$

Note that this dramatic increase of β has very little effect on the value of $\Delta'd$, a feature which is quite encouraging for our model. It should be pointed out that since $B_\phi = g_o/r_o$ = 1.0, the peaked total plasma beta $\beta \equiv 2p_o/[B_\phi^2(r_o) + B_p^2(r_2)]$ is 0.14 for β_v = .16, 0.5 for β_v = 1.0, and 0.99 for the case β_v = 100. That the average beta, β^*, is less than unity is due to the profile shape, with more flattened pressure profiles resulting in larger values of β^*.

We show in Fig. 6 the effect of varying the aspect ratio for $\lambda_p = -0.5$ and $\beta_v = 1.0$. It is clearly seen that Δ' increases with the aspect ratio. Toroidicity is thus a stabilizing influence here. For very large aspect ratio the slab-limit is approached and we can take advantage of the added simplicity to carry out an analytical comparison with the numerical results in this limit. Thus, in Eqs. (9), (10), and (11) we let $m/r \to k_y$, $k \to k_z$, $k_y^2 + k_z^2 \to k^2$, $r \to r_o + x$, $r_o \to \infty$, $\partial/\partial r \to \partial/\partial x$, $B_p \to B_z$, $B_\phi \to B_y$ and find

$$\frac{d}{dx}\, F^2\, \frac{d\xi_x}{dx} - k^2 F^2 \xi_x = 0 \quad , \tag{19}$$

and the singular points occur where $F \equiv k_z B_z - k_y B_y$ vanishes. Equation (19) could be derived directly from the primitive set of the MHD equation with the same result. Note that the pressure does not enter explicitly in this limit. It is convenient to write this equation in terms of the radial component of the perturbed magnetic field, $Q = iF\xi_x$ so that

$$\frac{Q''}{Q} - \frac{F''}{F} - k^2 = 0 \quad , \tag{20}$$

and

$$\Delta' = \frac{1}{Q}\left(Q_R' - Q_L'\right)_{r_s} \quad . \tag{21}$$

Equation (20) can be readily solved in the approximation where $k2 \to 0$. Since the term involving k^2 in Eq. (19) is stabilizing, this limit represents the most pessimistic case. The solution is

$$Q(x) = C_1 F(x) \int_a^x \frac{ds}{F^2(s)} + C_2 F(x) \quad , \tag{22}$$

where C_1 and C_2 are constants. If we take B_y to be constant, then the y component of the current is proportional to $F'(x)$, and the boundaries of the plasma are defined such that $F'(r_1) = F'(r_2) = 0$. Together with the boundary conditions that $Q(a) = Q(b) = 0$, we find

$$\Delta' = F'(r_s) \left[P \int_{r_1}^{r_2} ds \frac{F'(r_s) - F'(s)}{F^2(s)} + \frac{1}{F(r_1)} - \frac{1}{F(r_2)} \right]$$

$$+ F'^2(r_s) \left[\frac{b - r_2}{F^2(r_2)} + \frac{r_1 - a}{F^2(r_1)} \right] \quad , \tag{23}$$

where P denotes the principal value of the integral. The term involving the second pair of square brackets is positive definite and represents the stabilizing effect of the conducting wall.

In the slab limit the Grad-Shafranov equation becomes

$$y'' + \frac{r_o^2}{\psi_b^2} \frac{dp}{dy} = 0 \quad . \tag{24}$$

If we take the case where $p = p_o(1 - y)^2$, i.e., $\lambda_p = 0$, this becomes a linear inhomogeneous equation

$$y'' - \frac{2r_o^2\, p_o}{\psi_b^2} (1 - y) = 0 \quad , \tag{25}$$

with solution

$$y = 1 - \cos\left[\left(\frac{2r_o^2 p_o}{\psi_b^2}\right)^{1/2}(r - r_o)\right] \quad , \tag{26}$$

so that, with $d \equiv |r_1 - r_o| = \pi/2\ (\psi_b^2/2r_o^2 p_o)^{1/2}$, we find

$$B_z(r) = \begin{cases} -B_{oz} \sin \frac{\pi}{2} \left(\frac{r - r_o}{d}\right) , & |r - r_o| < d \\ \mp B_{oz} , & \pm(r - r_o) > d \end{cases} \tag{27}$$

$$j_y(r) = - B_z'(r) = \begin{cases} \frac{\pi B_{oz}}{2d} \cos \frac{\pi}{2} \frac{r - r_o}{d} , & |r - r_o| < d \\ 0 , & |r - r_o| > d \end{cases} \tag{28}$$

where $B_{oz} = (2p_o)^{1/2}$.

Substitution into Eq. (23) yields after some algebraic manipulation

$$\Delta' d = \frac{\pi^2 \delta}{2d} \frac{1 + \sin^2[\pi(r_s - r_o)/2d]}{\cos^2[\pi(r_s - r_o)/2d]} \quad , \tag{29}$$

where we have assumed the wall distance is equal on either side of the plasma i.e., $a - r_1 = b - r_2 = \delta$, and used the condition that

$$F(r_s) = -k_z B_{oz} \sin \left(\frac{\pi}{2} \frac{r_s - r_o}{d}\right) - k_y B_y = 0 \quad , \tag{30}$$

defines the position of the singular surface. Equation (29) shows that unless the wall touches the plasma, Δ' is always positive and becomes large as the singular surface moves towards the plasma edge. This is due to the fact that the resistive kink is driven by the current gradient rather than the current itself, and the presence of a finite B_y allows the singular surface to be located in the region of large gradient. We compared this result with our numerical method. In Table 1 we show the results of Δ' as given by Eq. (29) and also by a numerical case where we set the aspect ratio R = 1000.0, δ = 0.1, p_o = 0.08, $B_z(r_2)$ = −0.4 and r_o = 1000.0. The toroidal mode number m is 1.0 so that $k_y = 10^{-3} \ll 1$. We note that the agreement is quite satisfactory.

m = 0 Modes

If m = 0, the singular surface occurs where $B_p = 0$, i.e., on the null trace. The stability study of this mode should indicate whether or not the plasma will tend to break up into axisymmetric filaments. We thus carry out the numerical Δ' analysis with the singular surface fixed at $r = r_o$ for various value of k.

Setting m = o in Eqs. (9), (10), (11) and (12), the Euler-Lagrange equation can be written

$$(rQ_r')' - \left[\frac{1}{r}(1 + k^2r^2) - \frac{1}{r^2B_p^2}(r^2B_\phi^2)' - \frac{r^2}{B_p}\left(\frac{j_\phi}{r}\right)'\right] Q_r = 0 \tag{31}$$

where we have used the radial component of the magnetic field, $Q_r \equiv ikB_p\xi$, as the dependent variable and $j_\phi = -B_p'$.

Note that, since we are assuming that $r^2B_\phi^2$ is constant the driving term in Eq. (31) is independent of the magnitude of the pressure, so that the results below is independent of the plasma beta but of course depends on the shape of the profiles, aspect ratio and wall position.

We first do the case for the rounded current profile (λ_p = 0.0) with an aspect ratio of 5 (r_o = 10.0, r_2 = 12.0) and with several positions, δ, for the conducting shell. The numerical result is shown in Fig. 7a where we plot Δ'd versus k for various values of δ. As expected, a closely placed conducting wall is stabilizing. Also, Δ' decreases with increasing k which indicates that, like the ideal modes, the most unstable case for $m = o$ occurs when $k \to o$. This is consistent with the behavior of Δ' near r_o in Figs. 3-6 since k tends toward large values there. For the profile chosen, the wall must be located at the plasma edge to stabilize the modes with small k.

The results for the flat current model ($\lambda_p = -0.5$) are shown in Fig. 7b. There we see that the effect of moving the destabilizing current gradients away from the singular layer and out towards the wall substantially enhances the stability of the plasma. Here the wall can be one plasma radius away to achieve stability for all k.

We also infer from these results that, because of the greater stability at large k, the plasma will resist the tendency to break up into small axisymmetric filaments in the vicinity of the null trace.

An analytical comparison can also be carried out for the $m = o$ case. We have already assumed that rB_ϕ = constant. Now we construct an extremely flat current profile where

$$j_\phi = \begin{cases} j_o r & , \quad r_1 < r < r_2 \\ 0 & , \quad \text{otherwise} \end{cases} \quad , \tag{32}$$

This choice of j_ϕ is closely related to the flat current profile case, λ_p = -0.5 which is used previously since we have pointed out in the equilibrium section that flatness in the current really refers to the shape of the quantity j_ϕ/r rather than j_ϕ itself; this can be seen by examining Eq. (2) near the null trace, and is also a feature of equilibria of the Solov'ev type [16].

We have then for $r_1 < r < r_2$,

$$B_p(r) = -\frac{j_o}{2}\left(r^2 - r_o^2\right) \tag{33}$$

$$p(r) = p_o\left[1 - \frac{(r^2 - r_o^2)^2}{(r_2^2 - r_o^2)^2}\right] \tag{34}$$

with

$$j_o^2 = \frac{8p_o}{(r_2^2 - r_o^2)^2} \tag{35}$$

where we have used the equilibrium relation (12) and required that $p(r_2) = 0$. The requirement that $p(r_1) = 0$ gives

$$r_1^2 = 2r_o^2 - r_2^2 \quad . \tag{36}$$

Equation (36) is also the condition that $B_p(r_1) = -B_p(r_2) = (2p_o)^{1/2}$. The quantities j_ϕ, B_p, and p are sketched in Fig. 8.

Equation (31) thus reduces to the modified Bessel equation, with solution

$$Q_r(r) = CI_1(kr) + DK_1(kr) \tag{37}$$

with boundary condition $Q_r(a) = Q_r(b) = 0$, and, because of the discontinuity in j_ϕ at r_1 and r_2, the jump conditions which must be satisfied are

$$\left[Q_r'\right]_{r_2} = \frac{Q_r(r_2)}{B_z(r_2)}\, j_\phi(r_2)$$

$$[\, Q_r' \,]_{r_1} = - \frac{Q_r(r_1)}{B_z(r_1)} \, j_\phi(r_1) \quad ,$$

$$[\, Q_r \,]_{r_1} = [\, Q_r \,]_{r_2} = 0 \quad , \tag{38}$$

where $[Q]_r \equiv Q(r_+) - Q(r_-)$.

The constants C and D here have different values in the regions which are separated by the current discontinuities at r_1 and r_2. The expression for Λ' becomes, after some algebraic manipulation

$$\Lambda' \equiv \left[\frac{Q_r'}{Q_r} \right]_{r_o} = - \frac{1}{r_o} \, \frac{\alpha_\ell \beta_r - \alpha_r \beta_\ell}{(\alpha_r I_1 + \beta_r K_1)(\alpha_\ell I_1 + \beta_\ell K_1)} \Bigg|_{r_o} \tag{39}$$

where

$$\alpha_\ell = 1 - \frac{r j_\phi}{B_p} K_1 (I_1 - V_a K_1) \Bigg|_{r_1}$$

$$\beta_\ell = - V_a + \frac{r j_\phi}{B_p} I_1 (I_1 - V_a K_1) \Bigg|_{r_1}$$

$$\alpha_r = 1 - \frac{r j_\phi}{B_p} K_1 (I_1 - V_b K_1) \Bigg|_{r_2}$$

$$\beta_r = - V_b + \frac{r j_\phi}{B_p} I_1 (I_1 - V_b K_1) \Bigg|_{r_2}$$

and

$$V_a = \frac{I_1(ka)}{K_1(ka)}$$

$$V_b = \frac{I_1(kb)}{K_1(kb)}$$

In deriving Eq. (39) we have made use of the Wronskian relation

$$I_1K_1' - I_1'K_1 = -\frac{1}{kr} \quad .$$

To compare this analytical result with the numerical results we show the calculated values of Δ' in Fig. (9). The results are qualitatively predicted by examining Eq. (31) and Fig. 8. The strong stabilizing forces of the plasma associated with finite values of k compete against the destabilizing kicks of the current gradients at r_1 and r_2. Comparison with the flat current profile case of Fig. (7) shows very close agreement, the analytical model being the more stable case. This is reasonable since the destabilizing current gradient is further out at the edge of the plasma while remaining close to the stabilizing influence of the conducting wall, which in this case can be two plasma radii away for stabilization to all k.

IV. Conclusions

We have idealized a highly elongated tokamak configuration as a straight one-dimensional mid-section, held in equilibrium by appropriate two-dimensional end sections. In the limit of an infinitely long mid-section, we find stability against all ideal MHD modes if the toroidal field remains a vacuum field, the plasma being confined solely by the poloidal field, i.e., $\beta_p \sim 1$ and rB_ϕ = constant. The total plasma beta can, in principle, be arbitrarily close to unity for $B_p >> B_\phi$, regardless of the other equilibrium parameters. Finite-resistivity tearing modes limit the arbitrariness of these equilibrium parameters. The Δ' tearing analysis shows that small aspect ratio, a moderately close conducting shell, and a rather flat current profile are stabilizing influences. Moreover, it is found that the curves for Δ' are roughly independent of the plasma beta. The axisymmetric ($m = o$) resistive modes centered at the null trace appear to be less harmful than those ($m \neq o$) for which the tearing layer is allowed, by the presence of a finite toroidal field, to move into the region of larger current gradient. A nominal stable case is one in which the aspect ratio is 5, the wall at 20% of the minor radius, and the peak plasma beta is 99%. A tighter aspect ratio, a more careful fine-tuning of the current profile, and consideration of the actual stability threshold of Δ' should relax the restriction on the proximity of the conducting shell.

The stability of the double tearing region presents a special problem, which is not yet fully resolved. This region occurs on the small-major-radius side of the plasma, where the pressure-curvature effects are most favorable for stability, so that the threshold value of Δ' should be large and positive. A proper resolution of this question would require some treatment of the interior of the resistive layers, in order to continue the Euler-Lagrange solutions properly into the ideal MHD regions. This is a topic of current research.

In a more realistic tokamak configuration, the inner and outer magnetic flux surfaces would be connected through the two-dimensional ends, and a two-dimensional analysis is required to study the system rigorously. It should be pointed out, however, that the tokamak geometry possesses favorable average magnetic curvature, so that stability against low-beta flute-like modes should be at least as good as in the present analysis. Higher-β modes that are localized poloidally, i.e., ballooning modes, are susceptible to local driving forces on the large-major-radius side and in the end sections. Note, however, that in our long, thin approximation we achieved stability to all ideal modes; connecting the modes from the outer to the more stable inner section can only enhance the stability for modes localized in the outer straight section. The stability properties of modes localized in the end sections will depend upon the detailed end configuration; special tailoring of the plasma profile in these sections, with reliance on local shear effects [17] and non-Maxwellian features may be necessary for suppressing the destabilizing forces there. A detailed consideration of the end-section modes, which may limit the achievable values of β, will be deferred to a later paper.

ACKNOWLEDGMENT

Helpful discussions with Drs. F. W. Perkins, J. M. Greene, R. B. White, and other co-workers at Princeton are appreciated.

This work was supported by the U.S. Department of Energy, Contract No. DE-AC02-76-CHO3073.

Table

$r_o = 1000.0,\ r_2 = 1001.0,\ b = 1001.1,\ p_o = 0.08,\ g_o = 1000.0,\ B_p(r_2) = -0.4$

$r_s - r_o$	$\Lambda' d$ Numerical	$\Lambda' d$ Analytical
- 0.8	10.3	9.84
- 0.6	2.40	2.36
- 0.4	1.02	1.01
- 0.2	0.60	0.598
- 0.1	0.519	0.518
0.0	0.493	0.493
0.1	0.516	0.518
0.2	0.594	0.598
0.4	1.00	1.01
0.6	2.32	2.36
0.8	9.52	9.84

Appendix

We present here the details of the power series expansion of the coupled differential equations

$$\zeta' - G\xi = 0 \quad , \tag{A1}$$

$$F\,\xi' - \zeta = 0 \quad , \tag{A2}$$

about the point $r = r_s$. The functions $G(r)$, $F(r)$ are given in Eqs. (10) and (11).

Let $x = r - r_s$ and expand

$$F(r) = \sum_{m=0}^{\infty} F_m x^m \quad , \tag{A3}$$

$$G(r) = \sum_{m=0}^{\infty} G_m x^m \quad , \tag{A4}$$

$$\xi(r) = \sum_{n=0}^{\infty} \xi_n x^{n+\sigma} \quad , \tag{A5}$$

$$\zeta(r) = \sum_{n=0}^{\infty} \zeta_n x^{n+\sigma} \quad . \tag{A6}$$

The unknowns here are ξ_n, ζ_n, and σ, while G_m, F_m are obtained by Taylor expanding $G(r)$ and $F(r)$ about r_s. We solve here for ξ and ζ assuming arbitrary F_m, G_m and, later in this section, present the first few terms of the latter for our specific case.

Substitution of Eq. (A3)-(A6) into (A1) and (A2) gives the recursion relation for determining tha coefficients ξ_n and ζ_n:

$$\sum_{m=o}^{n} \left[(m+\sigma)(n+\sigma-1)\ F_{n-m} - G_{n-m-2}\right]\xi_m = 0$$

$$\zeta_{n-1} - \sum_{m=o}^{n} (m+\sigma)\ F_{n-m}\ \xi_m = 0 \tag{A7}$$

for each n. For our case we have $F_m = 0$ for $m < 2$ and $G_m = 0$ for $m < 0$, and r_s is thus a regular singular point of our differential equation. Note that we are avoiding the point where $\mu'(r_s) = 0$ since F_2 would vanish and this would lead to an essential singularity in the solution, and the assumptions of Eqs. (A5) and (A6) would be invalid.

The lowest order nontrivial equation occurs for n = 2 and it determines the indicial behavior

$$\sigma(\sigma+1)F_2 - G_o = 0 \quad , \tag{A8}$$

so that

$$\sigma_{\ell,s} = -\tfrac{1}{2} -,+ \ (-D_I)^{1/2} \quad , \tag{A9}$$

where $D_I = -\tfrac{1}{4} - G_o/F_2$ and the subscript ℓ , s indicates that appropriate root of σ which gives the large (ℓ) or small (s) solution respectively. We recognize here that Suydam's criterion is contained in Eq. (A9).

For the case where $G_o \neq 0$, higher values of n in Eq. (A7) gives

$$\xi_o = \text{Const.} \quad ,$$

$$\frac{\xi_1}{\xi_o} = - \frac{\sigma}{2} \left[\frac{\sigma(\sigma + 2) F_3 - G_1}{G_o} \right] \quad ,$$

$$\frac{\xi_2}{\xi_o} = - \frac{\sigma(\sigma + 3) \; F_4 - G_2 + [(\sigma + 1)(\sigma + 3) F_3 - G_1](\xi_1/\xi_o)}{(\sigma + 2)(\sigma + 3) F_2 - G_o} \quad ,$$

$$\frac{\zeta_o}{\xi_o} = 0 \quad ,$$

$$\frac{\zeta_1}{\xi_o} = \sigma \; F_2 = \frac{G_o}{\sigma + 1} \quad ,$$

$$\frac{\zeta_2}{\xi_o} = \tfrac{1}{2} \left[G_1 - \sigma^2 F_3 \right] \quad ,$$

$$\frac{\zeta_3}{\xi_o} = \sigma \; F_4 + (\sigma + 1) F_3 \frac{\xi_1}{\xi_o} + (\sigma + 2) F_2 \frac{\xi_2}{\xi_o} \quad , \text{etc.} \qquad \text{(A10)}$$

With the appropriate substitution of $\sigma = \sigma_{\ell,s}$ in these coefficients we construct the first few terms of the series expansion for the independent large, small solutions, ξ_ℓ and ξ_s, of Eq. (14). In the event that F_2 and G_o is such that $\sigma_s - \sigma_\ell$ is an integer, the relations in Eq. (A7) is inapplicable since the coefficients ξ_m are not determined. The situation where $G_o = 0$ is a special case of this occurrence and is treated below.

If $C_o = 0$ also, the indicial equation is

$$\sigma(\sigma + 1) = 0 \quad , \tag{A11}$$

and the solutions given by the roots of this equation are linearly dependent. For the root $\sigma = 0$ we find for the small solution, ξ_s

$$\xi_0 = \text{Const.} \quad ,$$

$$\frac{\xi_1}{\xi_0} = \frac{G_1}{2F_2} \quad ,$$

$$\frac{\xi_2}{\xi_0} = \frac{1}{6F_2}\left(G_2 - \frac{G_1}{2F_2}(3F_3 - G_1)\right) \quad ,$$

$$\xi_0 = \xi_1 = 0 \quad ,$$

$$\frac{\xi_2}{\xi_0} = \frac{1}{2} G_1 \quad ,$$

$$\frac{\xi_3}{\xi_0} = \frac{1}{3}\left(G_2 + \frac{1}{2}\frac{G_1^2}{F_2}\right) \quad , \quad \text{etc} \tag{A12}$$

The other linearly independent solution, ξ_ℓ, can be constructed from ξ_s in the usual manner:

$$\xi_\ell(r) = \xi_s(r) \int^r \frac{dr'}{F(r')\xi_s^2(r')}$$

$$= -\frac{1}{\xi_o F_2}\left[\frac{1}{x} + \frac{\xi_1}{\xi_o} \cdot \left(c_2 + \frac{\xi_2}{\xi_o}\right) x + \dots\right.$$

$$\left. + c_1 \ln |x| \left(1 + \frac{\xi_1}{\xi_o} x + \frac{\xi_2}{\xi_o} x^2 + \dots\right)\right] \qquad \text{(A13)}$$

where

$$c_1 = \frac{F_3}{F_2} + 2\frac{\xi_1}{\xi_o} \quad ,$$

$$c_2 = \frac{F_4}{F_2} + \frac{\xi_1^2}{\xi_o^2} + 2\frac{\xi_2}{\xi_o} + 2\frac{F_3}{F_2}\frac{\xi_1}{\xi_o} - c_1^2 \quad .$$

The corresponding expansion for the large component, ξ_ρ, is

$$\xi_\rho = F \xi_\rho'$$

$$= \frac{1}{\xi_o}\left\{1 - 2\frac{\xi_1}{\xi_o} x - \left[3\frac{\xi_2}{\xi_o} - \frac{\xi_1^2}{\xi_o^2} + \frac{F_3}{F_2}\frac{\xi_1}{\xi_o}\right] x^2\right.$$

$$\left. - c_1 x^2 \ln |x| \left[\frac{\xi_1}{\xi_o} + \left(\frac{F_3}{F_2}\frac{\xi_1}{\xi_o} + 2\frac{\xi_2}{\xi_o}\right) x + \dots\right]\right\} \quad . \qquad \text{(A14)}$$

The subscript s on the ξ_n's in Eqs. (A12)-(A14) have been dropped since the meaning there is unambiguous. We note that since G_o is proportional to p', the cases where the plasma is pressureless or when the singular point lies where p' = 0 (as in our m = 0 case), must be analyzed by using the series expansion given by these equations.

For our case the first few terms on the Taylor expansion of $F(r)$ and $G(r)$ about r_s are calculated as follows. We let

$$\hat{F} = kB_p - \frac{m}{r} B_\phi \quad ,$$

$$\bar{F} = krB_p + m B_\phi \quad ,$$

$$H = r^3\lambda \quad ,$$

$$\lambda = (k^2r^2 + m^2)^{-1} \quad ,$$

then

$$F = H \hat{F}^2 \quad ,$$

and

$$G = 2k^2r^2\lambda p' + r\hat{F}^2(1 - \lambda) + 2k^2r^2\lambda^2 \hat{F} \bar{F} \quad .$$

Hence at $r = r_s$ we have

$$F_o = F_1 = 0 \quad ,$$

$$F_2 = \frac{F''}{2} = H \hat{F}'^2 \quad ,$$

$$F_3 = \frac{F'''}{6} = H \hat{F}'^2 \left(\frac{\hat{F}''}{\hat{F}'} + \frac{H'}{H} \right) \quad ,$$

$$F_4 = \frac{F''''}{24} = H \left(\frac{\hat{F}''^2}{4} + \frac{\hat{F}' \hat{F}'''}{3} \right) + \frac{H'' \hat{F}'^2}{2} + H' \hat{F}' \hat{F}'' \quad ,$$

$$G_o = 2k^2r^2\lambda p' \quad ,$$

$$G_1 = G' = 2k^2 r\left[r\lambda p'' + r\lambda^2 \hat{F}' \bar{F} + p'\left(r\lambda' + 2\lambda\right)\right] \quad ,$$

$$G_2 = \frac{1}{2} G'' = k^2 r\left[r\lambda p''' + 2p''\left(r\lambda' + 2\lambda\right) + p'(r\lambda'' + 4\lambda')\right.$$

$$\left. + r\lambda^2 \hat{F}'' \bar{F} + 2r\lambda^2 \hat{F}' \bar{F}' + 6\lambda^2 \hat{F}' \bar{F} + 4r\lambda\lambda' \hat{F}' \bar{F} \right]$$

$$+ 2k^2 p'\lambda + r \hat{F}'^2 \left(1 - \lambda\right) \quad . \tag{A15}$$

It is relevant to determine the accuracy to which the coefficients, A and B, are calculated in Eq. (16) by using the truncated series generated here.

Let

$$f = f^o + \hat{f} \quad , \tag{A16}$$

where f^o is any truncated quantity and $\hat{f}$ the remainder. Equation (16) gives

$$A^o = \frac{\xi \zeta_s^o - \zeta \xi_s^o}{W^o} \quad ,$$

$$B^o = -\frac{\zeta \xi_\ell^o - \xi \zeta_\ell^o}{W^o} \quad , \tag{A17}$$

where

$$W^o \equiv \xi_\ell^o \zeta_s^o - \zeta_\ell^o \xi_s^o \quad . \tag{A18}$$

Using Eq. (A16) for ξ and ζ in Eq. (14) and substituting these in Eq. (A17) gives the error in A and B:

$$\tilde{A} = A - A^{o} = A\,\frac{\tilde{\zeta}_{\ell}\,\xi_{s}^{o} - \tilde{\xi}_{\ell}\,\zeta_{s}^{o}}{W^{o}} + B\,\frac{\tilde{\zeta}_{s}\,\xi_{s}^{o} - \tilde{\xi}_{s}\,\zeta_{s}^{o}}{W^{o}} \quad , \qquad (A19)$$

$$\tilde{B} = B - B^{o} = B\,\frac{\tilde{\xi}_{s}\,\zeta_{\ell}^{o} - \tilde{\zeta}_{s}\,\xi_{\ell}^{o}}{W^{o}} + A\,\frac{\tilde{\xi}_{\ell}\,\zeta_{\ell}^{o} - \tilde{\zeta}_{\ell}\,\xi_{\ell}^{o}}{W^{o}} \quad . \qquad (A20)$$

The tendency for the contribution of the small solution to be masked by the large one is manifested in the last term of Eq. (A20), which is generally the largest of these error terms. Retaining only this term, and assuming that the series given by Eq. (A10) has n terms, we find for the situation when $G_o \neq 0$:

$$\tilde{B} \sim O(x^{\lambda}) \quad ,$$

where

$$\lambda = 2\sigma_{\ell} + 1 + n \quad = \quad -2(-D_I)^{1/2} + n \quad .$$

Usually, $0 < -D_I \approx 1/4$, so that n = 2 gives reasonably accurate results. However, near the point where F_2 vanishes, D_I gets large and negative and consequently n must be large enough to have $\lambda > 0$. Alternatively, if n is fixed, acceptable results can be obtained only if the singular surface is some minimum distance from the point where F_2 vanishes.

If $G_o = 0$, we have

$$\tilde{B} \sim \frac{1}{F_2}\,\frac{\tilde{\zeta}_{\ell}}{x} + \tilde{\xi}_{\ell} \quad ,$$

so that, to realize errors of $x\ell n|x|$, x, or $x^2\ell n|x|$ we must have respectively n = 3, 4, or 5 in Eq. (A13) and n = 2, 3, or 4 in Eq. (A14).

A necessary check of the accuracy of the calculations is to compare the Wronskian relation, W^o as calculated by Eq. (A18) with the known value, $W = 1.0$.

REFERENCES

[1] TODD, A. M. M., MANICKAM, J., OKABAYASHI, M., CHANCE, M. S., GRIMM, R. C., GREENE, J. M., JOHNSON, J. L., Nucl. Fusion 19 (1979) 743.

[2] BECKER, G., LACKNER, K., in Plasma Physics and Controlled Nuclear Fusion Research 1976 (Proc. 6th Conf. Berchtesgaden, 1976) Vol. II, IAEA Vienna (1977) 401.

[3] CHANCE, M. S., GREENE, J. M., GRIMM, R. C., JOHNSON, J. L., Nucl. Fusion 17 (1977) 65.

[4] GROSSMAN, W., TATARONIS, J. A., WEITZNER, H., Phys., Fluids 20 (1977) 239.

[5] BERGER, D., BERNARD, L. C., GRUBER, R., TROYON, F., in Plasma Physics and Controlled Nuclear Fusion Research 1976 (Proc. 6th Int. Conf. Berchtesgaden, 1976) Vol II, IAEA Vienna (1977) 411.

[6] DOBROTT, D. R., MILLER, R. L., Phys. Fluids 20 (1977) 1361.

[7] WESSON, J. A., Nucl. Fusion 18 (1978) 87.

[8] GRIMM, R. C., DEWAR, R. L., MANICKAM, J., CHANCE, M. S., Bull. Am. Phys. Soc. 8 (1980).

[9] NEWCOMB, W. A., Ann. Phys. 10 (1960) 232.

[10] SUYDAM, B. R., 2nd Int. Conf. Peaceful Uses At. Energy (Proc. Conf. Geneva, 1958), 31, UN New York (1958) 157.

[11] FURTH, H. P., KILLEEN, J., ROSENBLUTH, M. N., Phys. Fluids 6 (1963) 459.

[12] GLASSER, A. H., GREENE, J. M., JOHNSON, J. L., Phys. Fluids 18, (1975) 875, Phys. Fluids 19, (1976) 567.

[13] BERNSTEIN, I. B., FRIEMAN, E. A., KRUSKAL, M. D., KULSRUD, R. M., Proc. Roy. Soc., Ser. A 244, (1958) 17.

[14] BORIS, J., WINSOR, N., Princeton Plasma Physics Lab. 652 (1970).

[15] FURTH, H. P., RUTHERFORD, P. H., SELBERG, H., Phys. Fluids 16 (1973) 1054.

[16] SOLOV'EV, L. S., Zh. Eksp. Teor. Fiz 53 (1967), 626; Sov. Phys. JETP 26 (1968) 400.

[17] GREENE, J. M., CHANCE, M. S., Nucl. Fusion 21 (1981) 453.

Figure Captions

Fig. 1. A sketch of the central one-dimensional region showing the plasma and conducting shell (a). The poloidal magnetic field B_p reverses across the null trace (dotted line), and the plasma is contained within the dashed vertical lines. The required terminations at the two-dimensional ends are not shown. Figure 1(b). shows, in arbitrary units, the profiles of the pressure, p, pitch, μ and the toroidal and poloidal magnetic fields.

Fig. 2. The pressure and current profile shapes for the peaked (λ_p = 1.0), rounded (λ_p = 0.0), flat (λ_p = -0.5), and hollow (λ_p = -1.0) models. These shapes are the ones used for the results shown in Fig. 4b.

Fig. 3. The effect of the position of the conducting shell on $\Delta'd$ for β_v = 0.16 (a) and β_v = 0.5 (b), with aspect ratio R = 5. The plasma is enclosed within the dashed vertical lines and the walls are depicted by the hashed vertical lines.

Fig. 4. The effect on $\Delta'd$ due to changes in the profile shape. The shapes, which correspond to the values of λ_p shown in the figure, are shown in Fig. 2. β_v = 0.16 (a) and 0.5 (b). The wall position is fixed at 0.2d, and the aspect ratio, R, is 5.

Fig. 5. The effect of varying β is shown for the flat current case (λ_p = -0.5) and the wall held at 0.2d, with R = 5. The peak β value is shown by each curve, and the corresponding β_v and β^* are given in the text.

Fig. 6. Here, the aspect ratio R is varied, with the wall kept at 0.2d and β = 0.5. For the upper curve, R = 5 (r_o = 10, r_2 = 12), the center curve R = 10 (r_o = 10, r_2 = 11) and for the lower curve, R = 100 (r_o = 10, r_2 = 10.1).

Fig. 7. Δ'd as a function of k for the m = 0 modes. The numerical values shown on the separate curves denote the respective positions of the conducting shell. The results for the rounded (a) and flat (b) profiles are shown. The aspect ratio is 5.

Fig. 8. A sketch of the pressure, current and poloidal field profiles for the "extremely" flat current model.

Fig. 9. Plots of Δ'd as in Fig. 7, but for the analytical model of the "extremely" flat current profile shown in Fig. 8.

Table 1. A comparison of the numerical result with the analytical calculation for a very large aspect ratio case (slab limit). The table shows Δ'd as a function of the distance, $x_s - x_o$, of the singular layer from the null trace at x_o.

#81T0136

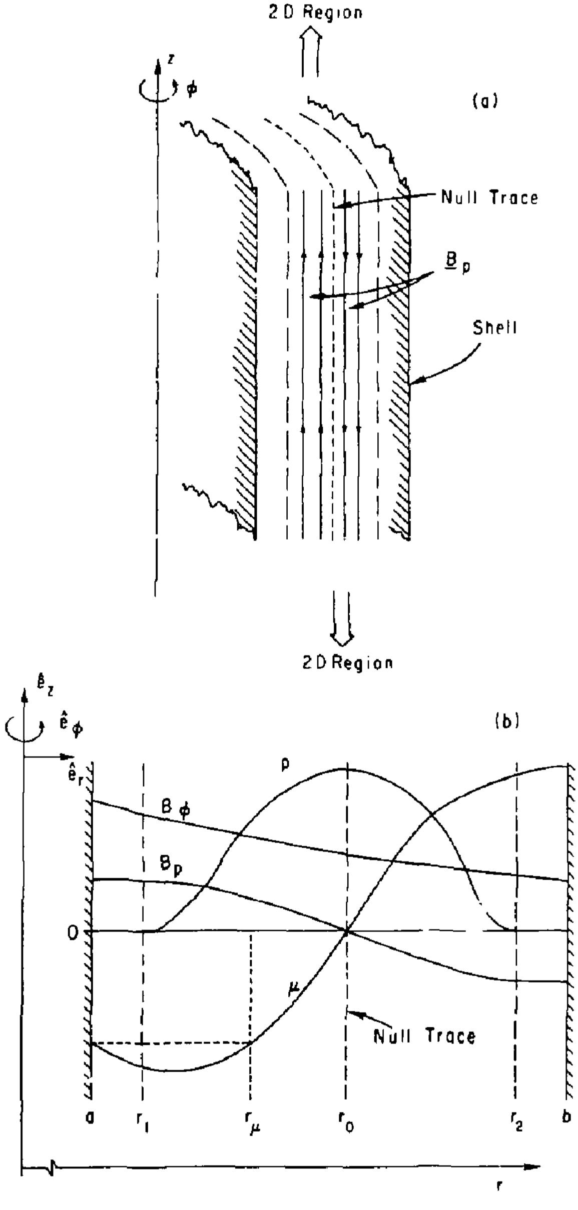

Fig. 1

81T0141

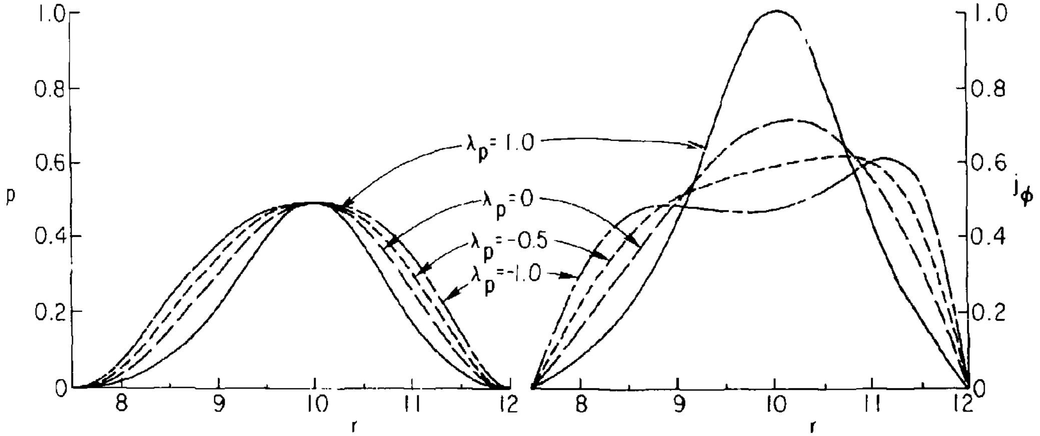

Fig. 2

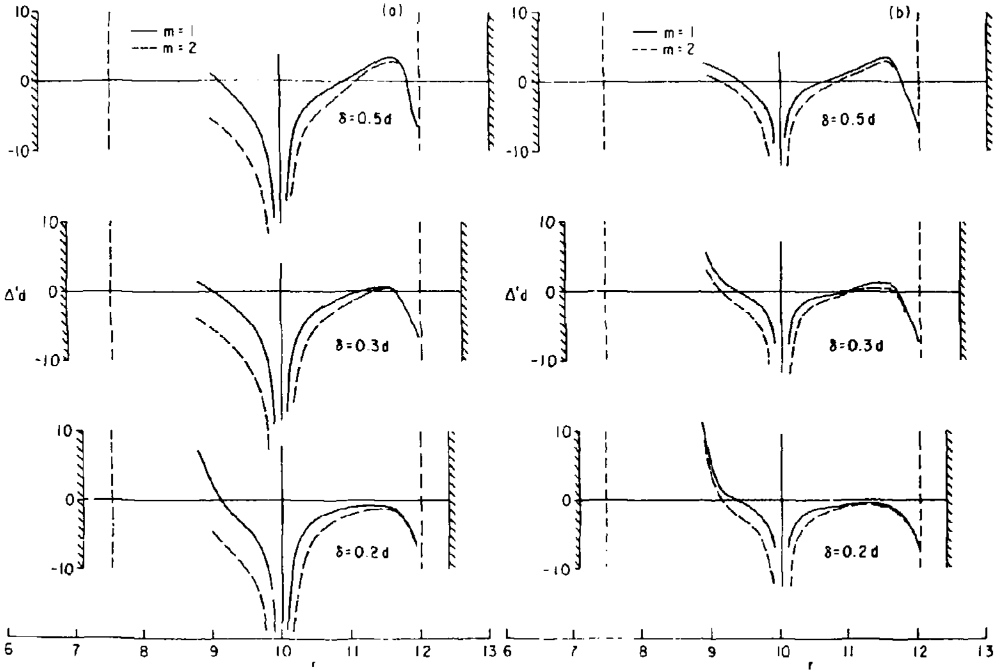
(a)
(b)
m = 1
m = 2
δ=0.5d
δ=0.3d
δ=0.2d
Δ'd
10
0
-10
6
7
8
9
10
11
12
13
r

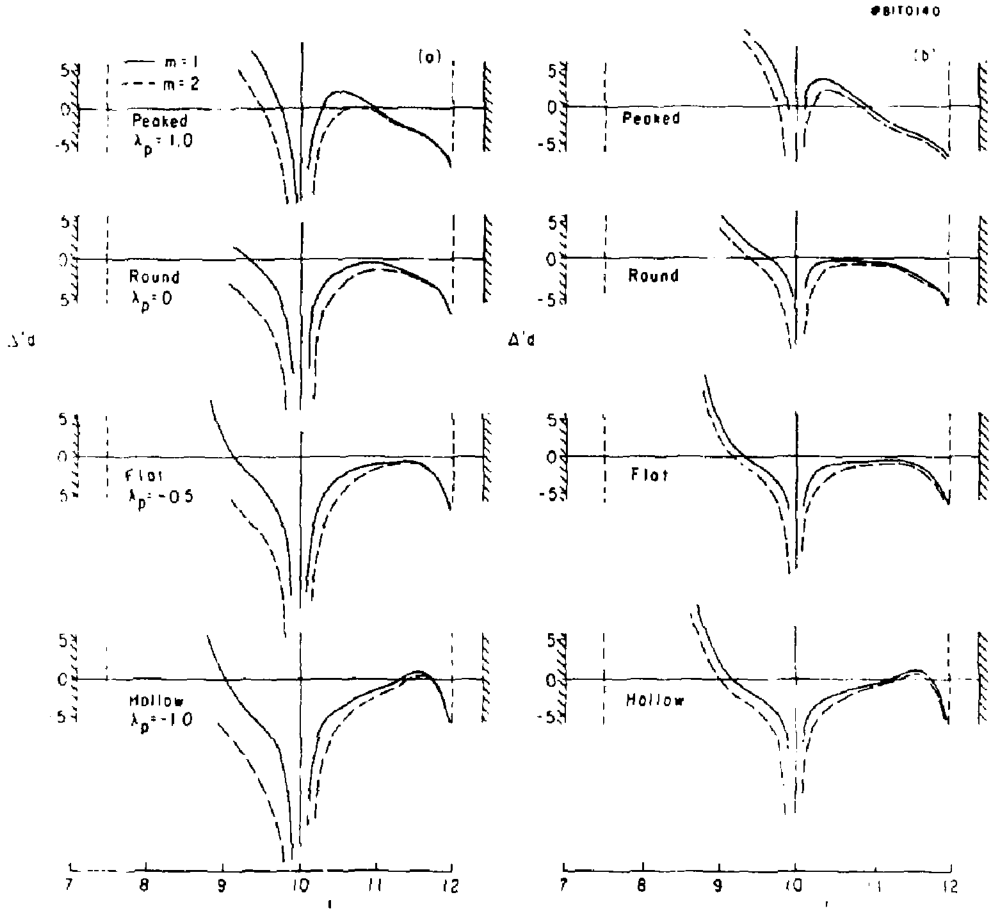
#81T0140
m = 1
m = 2
(a)
(b)
Peaked
λ_p = 1.0
Round
λ_p = 0
Flat
λ_p = -0.5
Hollow
λ_p = -1.0
Peaked
Round
Flat
Hollow
$\Delta'a$
$\Delta'a$
5
0
-5
7
8
9
10
11
12
r

Fig. 4

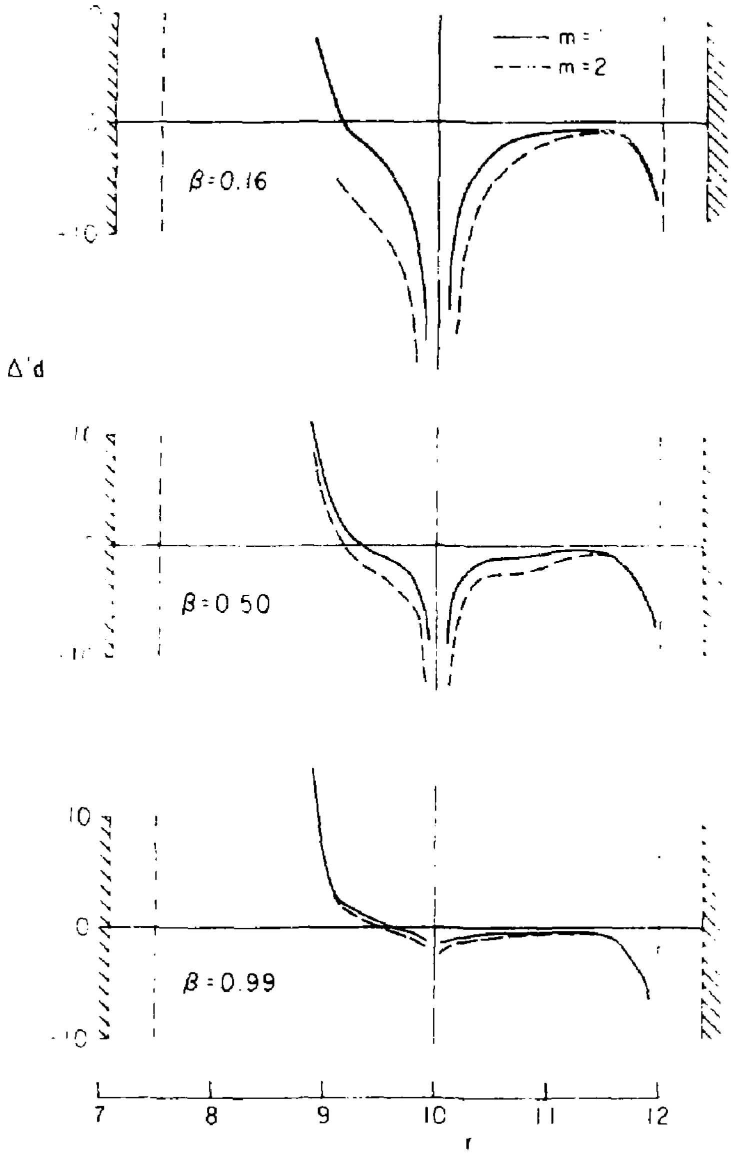

Fig. 5

81T0134

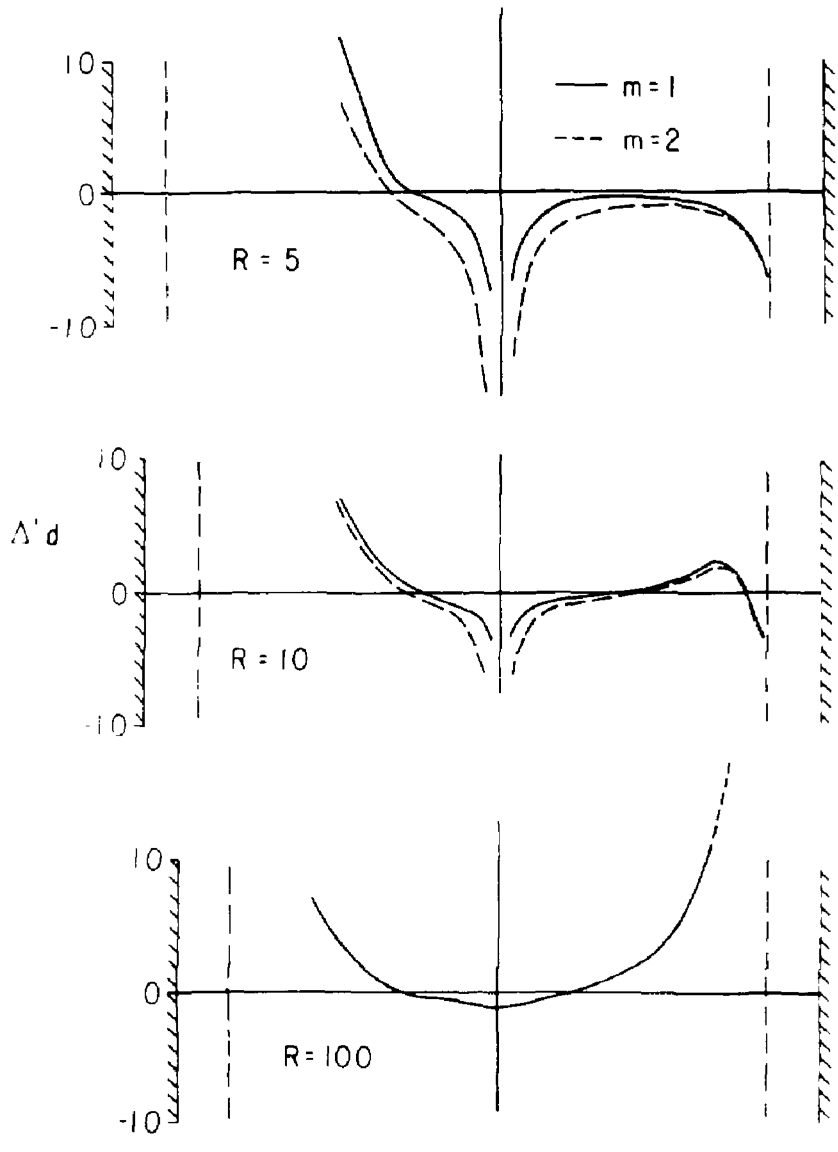

Fig.

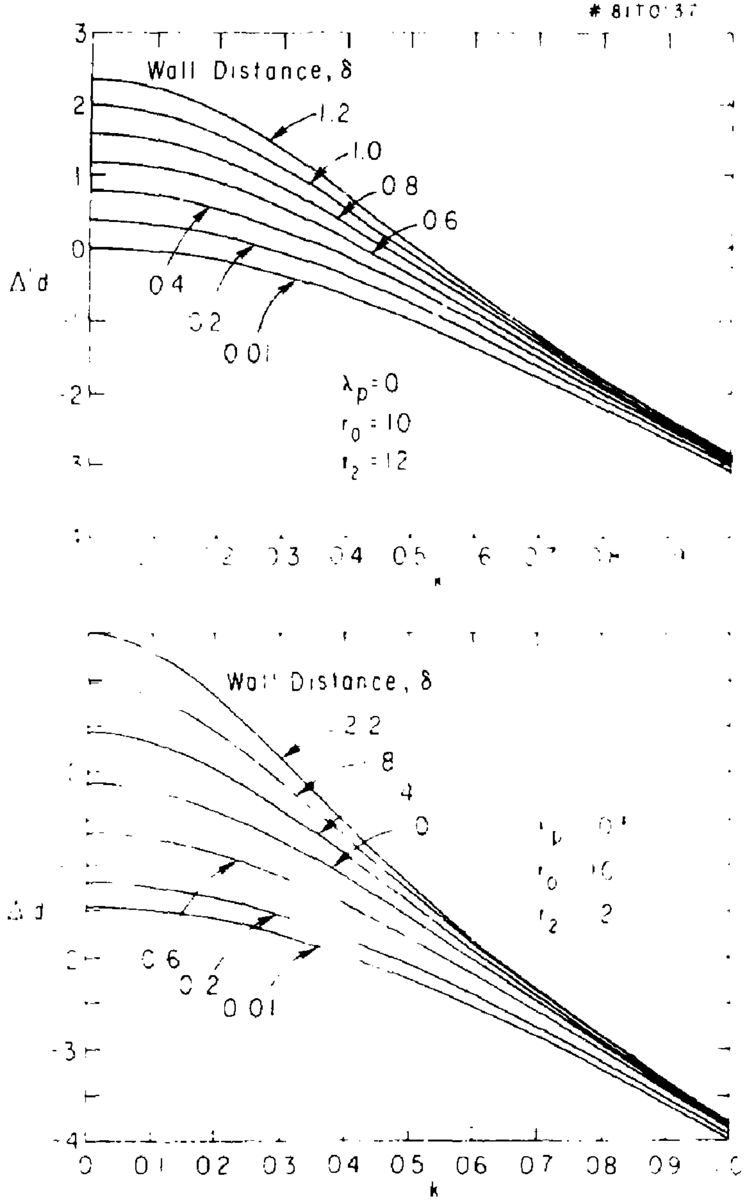

81TO'37
Wall Distance, δ
1.2
1.0
0.8
0.6
0.4
0.2
0.01
$\lambda_p = 0$
$r_0 = 10$
$r_2 = 12$
Δ'd
Wall Distance, δ
0.6
0.01

Fig. 7

81T0133

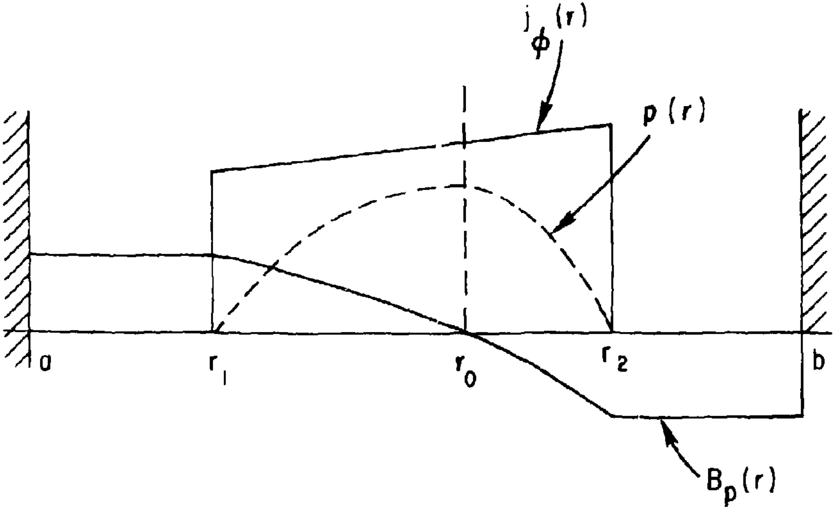

#81T0138

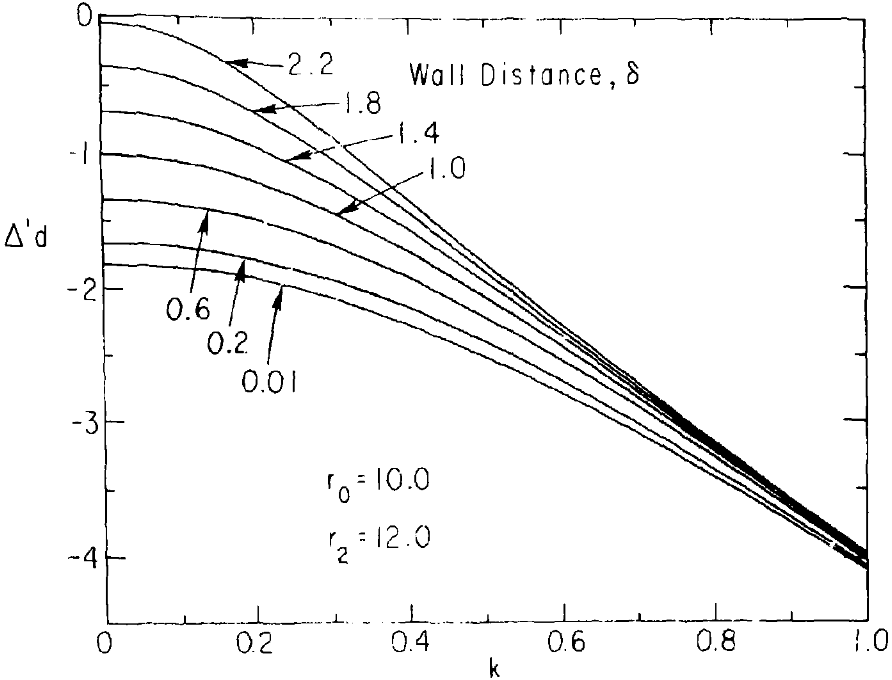
Wall Distance, δ
2.2
1.8
1.4
1.0
0.6
0.2
0.01
Δ'd
k
r0 = 10.0
r2 = 12.0
0
-1
-2
-3
-4
0
0.2
0.4
0.6
0.8
1.0